IRAQI Academic Scientific Journals
Samarra Journal of Pure and Applied Science
SJPAS
www.sjpas.com
p ISSN: 2663-7405
e ISSN: 2789-6838

Effect of copper content on the structural properties of the $Cu_xCo_{1-x}Fe_2O_4$ Nanostructured Spinel Ferrite Based on Williamson-Hall Analysis

Maram J. Hassen[1], Nezar Ismat Seno[2], Mazin A. Alalousi[3] and Jamal M. Rzaij[3]*
1- Computer Science Department., College of Basic Education, Al-Mustansiriyah University, Iraq
2- Renewable Energy Research Centre, University of Anbar, Iraq
3- Department of Physics, College of Science, University of Anbar, Ramadi, Iraq

https://doi.org/10.54153/sjpas.2024.v6i4.950

Article Information
Received: 02/07/2024
Revised: 05/08/2024
Accepted: 08/08/2024
Published:30/12/2024

Keywords:
Cu-Co ferrite, spinal ferrite, Williamson-Hall, structural properties, nanoferrite.

Corresponding Author
E-mail: sc.jam72al@uoanar.edu.iq
Mobile:

Abstract
The current study investigated the effect of replacing cobalt ions (Co^{+2}) with copper ions (Cu^{+2}) to modify the physical properties of the $Cu_xCo_{1-x}Fe_2O_4$ nanocomposite at x-values of 0, 0.05, 0.1, and 0.15 deposited using the sol-gel combustion method. Structural analysis was performed using X-ray diffraction patterns and the Williamson-Hall method. The patterns revealed polycrystalline ferrites without distinct peaks associated with copper. The dominant phase of crystal growth was toward the (311) diffraction peak, with a noticeable shift of the diffraction peaks toward the lower diffraction angle with increasing x content. It was observed that the crystal lattice constant decreased while the intensity of the diffraction peaks increased with increasing x-content. The study showed that the prepared film has a lattice constant of 0.8361 ± 0.005 nm with an X-ray density of 5.347 g/cm^3 for the sample with x = 0.15. In addition, crystallite size varied from 10.74 nm to 20.46 nm, and microstrains from -0.00255% to -0.00309% were observed with varying x-content ratios.

Introduction:

Chemically stable magnetic nanomaterials type $A^{2+}B_3^{2+}O_4$ (A= Fe, Co, Mn, Ni, Zn, and Cu) and B such as Fe [1]. These materials have a spinal structure [2], and they have attracted researchers' attention due to their vast potential in numerous applications[3], including magnetic recording media, antenna rods [4], biomedical [5], relays, transformers, and microwave isolators [6]. Cobalt ferrite ($CoFe_2O_4$) nanostructure is a material with a wide range of magnetic coactivity (233-2002 Oe) and has a modest magnetization (47-56 emu/g). It demonstrates stability in both physical and chemical properties [7]. Cobalt ferrite generally has an inverse spinel structure. The typical structure of cobalt ferrite is an inverse spinel arrangement. Within this arrangement, both the A and B sites are comprised of a combination of Co^{+2} and Fe^{+3} cations. Nevertheless, it is well recognized that substantial propparens of Co^{+2} ions are located at the B-site, with the remaining ions being parent at the A-site. The

distribution of cations is as follows: CO^{+2} ins occupy the octahedral sites (B-site), when Fe^{3+} ions are evenly distributed between the tetrahedral and octahedral sites. The cation distribution parens be represented by $\left[Co_{1-\delta}^{+2}Fe_{\delta}^{+3}\right]_A\left[Co_{\delta}^{+2}Fe_{2-\delta}^{+3}\right]_B O_4^{-2}$. The symbol δ represents the proportion of tetrahedral sites that are occupied by Fe^{3+} ions, which is also known as the degree of inversion [8]. Typically, the magnetic characteristics of cobalt ferrite are controlled by adjusting the temperature or annealing time. Nevertheless, achieving a clear correlation between microstructure and magnetic response is challenging due to variations in cation redistribution [9]. However, numerous investigations have demonstrated considerable alterations in the magnetic characteristics of cobalt ferrite [5, 10–12]. Besides unique structural, magnetic, and optical features, it has attracted considerable attention applicable in electronic industries [13, 14], MRI, magnetic hyperthermia [15], gas sensors, microwaves, magnetic fluids, recording media, and power transformers applications [11]. The Large-scale applications of $CoFe_2O_4$ nanoferrite led to utilizing various methods such as sol-gel [16], polyol method [12], solvothermal method [17], combustion and co-precipitation [18].

The magnetic and structural properties of Co ferrite depend on the particle shape and purity [19]; the incorporation of elements such as Zn, Mn, Cu, and Ni can further improve these features [20]. Copper doping results in the exchange of sites between Co^{+2} and Cu^{2+} ions [21] as Co^{+2} ions are transformed from octahedral sites to tetrahedral sites. Here, Crystal symmetry decreases inversely with increasing copper ion concentration due to the Jahn-Teller effect [22], which arises from the disparity in magnetic moments and ionic radii of cobalt and copper ions. Additionally, it has been observed that higher copper ion concentrations result in a reduction of the ferrite cell parameter [21]. These changes lead $CuCoFe_2O_4$ to be classified as inverse spinals [23]. This gives these materials unique magnetic and electronic properties due to the distribution of $Fe^{(+2\text{ and }+3)}$ ions between tetrahedral and octahedral sites, making them suitable for numerous applications mentioned earlier [24].

Investigation into the $Cu_xCo_{1-x}Fe_2O_4$ system has been started for a minimum over the last ten years. Therefore, Numerous studies have been carried out to assess the impact of Cu^{+2} on the structural system of the $Cu_xCo_{1-x}Fe_2O_4$ ferrite system, where Singh et al. [19] synthesized Copper-substituted cobalt ferrite nanoparticles (Co1-xCuxFe2O4, x = 0.01, 0.03, 0.05, 0.07, 0.09 annealed at 700°C for 1h) employing the citrate precursor. They annealed powders at 700 C and that displayed a cubic spinel structure, observing variations in particle size, lattice constant (8.376, 8.371, 8.362, 8.385, 3.387)Å, magnetization, and retentivity with increased Cu content. Then, Jnaneshwara et al. [25] synthesized $Co_{1-x}Cu_xFe_2O_4$ (X=0, 0.1, 0.2, 0.3, 0.4, and 0.5), examining magnetic, conductivity, and structural properties. They observed a decrease in lattice parameters (8.39, 8.4109, 8.4109, 8.4019, 8.4109, and 8.3910) Å and an increase in X-ray density (5.3850, 5.1884, 5.2054, 5.2224, 5.2394 and 5.2564) (g/cm^3). Batoo et. al [22] used a different compensation method to study $Cu_xCo_{1-x}Fe_2O_4$, the lattice linear expansion induced (a=8.3834, 8.3835, 8.3837 8.3839, 8.3840 and 8.3843) Å by introducing Cu^{+2} ions into the CoFe2-xCuxO4 (x=0.0, 0.1, 0.2, 0.3, 0.4, and 0.5) crystal structure instead of Fe^{+3} accordingly a Cu^{+2} content. Ghosh and Mukherjee [26] investigated the structural and magnetic properties of polycrystalline Cu-substituted cobalt ferrite ($Cu_xCo_{1-x}Fe_2O_4$: x = 0.00, 0.15, 0.30, 0.45, 0.60) nanoparticles synthesized via chemical co-precipitation. X-ray diffraction confirmed the samples were single phase, with mean crystallite sizes ranging from 44-65 nm calculated using Scherrer's formula. $CuCoFe_2O_4$@Chitosan was synthesized by

Nasiri et al. [27] via a microwave-enhanced chemical method for industrial pollutant adsorption with 82.16% after four cycles of adsorption-desorption, while Anju et al. [28] prepared CuxCo1−xFe2O4 (x = 0.33, 0.67, 1)-(rGO)-(TPU) nanocomposites for effective EM interference shielding through melt-mixing with a micro compounded, they found the crystallite size be found (55.1, 49.6 and 39.4) Å. Alahmari et al. fabricated Cu–Co ferrite nanofibers via electrospinning for potential anticancer applications against HCT-116 and HeLa cells [20]. Saleem et al. also noted decreased lattice parameters with higher Cu^{+2} content in $Cu_{1-x}CoxFe_2O_4$ (X= 0.04, 0.08, and 0.12) [29].

This study investigates how varying copper content affects the structural properties of Cu-Co spinel ferrite. Copper substitution levels of x = 0.05, 0.10, and 0.15 were examined using X-ray diffraction and Williamson-Hall analysis.

Materials and methods

Synthesis of ferrites

Salt solutions of all citric acid $HOC(COOH)(CH_2COOH)_2$, Fe $(NO_3)_3.9H_2O$, Co $(NO_3)_2.6H_2O$, Cu $(NO_3)_2.2H_2O$ and citric acid $HOC(COOH)(CH_2COOH)_2$ were prepared by (3, 2, 1, 1) M respectively in 40 ml of deionized water through continuous stirring for 30 minutes until a clear solution formed for each. Then, they maxed by (2:1:0), (2:0.95:0.05), (2:0.9:0.1), and (2:0.85:0.15) Vol. %. Next, the citric acid solution is added carefully to the mixed solution on the magnetic stirrer without heat, followed by ammonia drops gradually added until reaching the desired pH level of (7). After that, they are heated until the mixture temperature reaches 90^O until the mixture becomes gelatinous, then the mixer is stopped, and heating continues until the gel ignites automatically and completely. The resulting ferrite is left to cool and ground using a mortar. After that, the resulting ferrite powder is placed in the oven for two hours at a temperature of 600°C

Characterization

The structural characteristics of ferrite powder were investigated using X-ray diffraction (XRD) at room temperature. The diffraction angle was scanned from 10 to 80 degrees, with a scanning speed of 0.05 degrees per second. Cu-Kα radiation with a wavelength of 1.5405 Å was used. The Bragg's relation was employed to calculate the lattice parameter (a) of a cubic spinel lattice using Equation (1) [4]:

$$a = \frac{\lambda}{2\,sin\theta}\sqrt{h^2 + k^2 + l^2} \quad \ldots\ldots\ldots\ldots (1)$$

where θ stands for Bragg's position, and (hkl) denotes the Miller indices.

Crystallite size is commonly determined using the Debye –Scherrer equation under ideal conditions. But in the process of creating crystals, small distortions in the grid structure occur due to either expansion or compression. These distortions cause a change in the grid's dimensions. The expansion or compression happens because the atoms in the grid move differently from their original positions [30]. Therefore, the X-ray density (d_x) (g/cm^3)values can be predicted through the Equation (2) [31].

$$d_x = \frac{ZM}{N_A a^3} \quad \ldots\ldots\ldots\ldots (2),$$

where Z, M, N_A, and a^3 are the number of molecules per unit cell, for Cu-Co ferrite is (Z=8), the molecular weight, Avogadro's number, and volume of the cell, respectively.

However, to account for strain effects that can alter the crystallite size value, the Williamson-Hall method is often utilized for necessary adjustments [32]. The total stress-induced and volume stress at *the hkl* diffraction peak can be expressed using Equation (3) [33].

$$\beta_{hkl} = (\beta_{hkl})D_{hkl} + (\beta_{hkl})\varepsilon \text{ ..... (3)},$$

where D_{hkl} (nm) is the crystallite size, $\beta_{hkl}$is the full width at half maximum (FWHM) of the diffraction peaks and ε is the strain.

The crystallite size was estimated through the Williamson-Hall (W-H) relation (Equation (4)) [34].

$$cos\theta.\beta_{hkl} = \left(\frac{A\lambda}{D_{hkl}}\right) + (4\varepsilon\, sin\,\theta) \text{ ..... } (4)$$

where (A) denotes the dimensionless shape factor (0.89) and θ (rad) is the diffraction angle. In addition, the quantitative phase measurements were achieved using the reference intensity ratio (RIR) method.

Result and Discussion

The XRD patterns shown in Fig.1 indicate that the Co ferrite and Cu-Co ferrite exhibit polycrystalline structures with cubic symmetry, confirming their crystallization consistent with the ICDS 98-009-8553 card. The dominant peaks of all x ratios were recorded at 2θ= (35.259, 35.363, 35.386, and 35.582) ^{o} with the preferred orientation toward the (311) diffraction peak that was used in calculating the parameters. Despite the addition of copper ions, no distinct peaks related to them were observed, most likely due to their restricted quantity [35, 36]. Nevertheless, a clear influence on the values of the diffraction pattern parameters was detected as shown in (x=0.05, 0.1, and 0.15) patterns.

The lattice parameter (a) is estimated utilizing Equation (1), where decreases as an increase of (Cu^{+2}) ions from 8.435 Å for (x=0) to 8.361 Å for (x=0.15). According to Vegard's law, there is a linear relation between the lattice parameter and the concentrations of compounds in solid solutions [37], where (Cu^{+2}) with an ionic radius of 0.72 Å substitutes (Co^{+2}) with an ionic radius of 0.74 Å. This substitute leads to reduce the lattice parameter has occurred [38] as illustrated in Fig. 2a and, tabulated in Table (1).

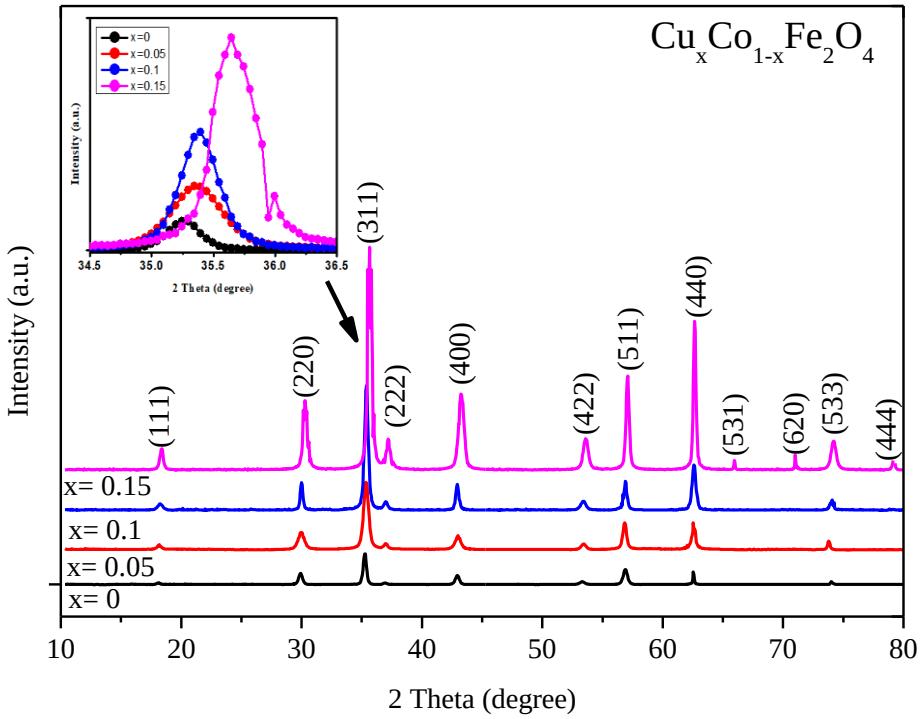

Fig.1 XRD patterns of the prepared Cu-Co ferrites.

Upon evaluating dx values against the substitution values for Cu^{+2} from Equation (2), it is evident that there is a near-linear increase of the X-ray density (d_x), depicted in Fig. 2b. The rise in X-ray density due to Cu^{2+} doping is because of the greater density of Cu^{+2} ions (8.92 g/cm^3 [39]) in comparison to the substituted ions such as Co^{+2} (8.86g/cm^3 [40]).

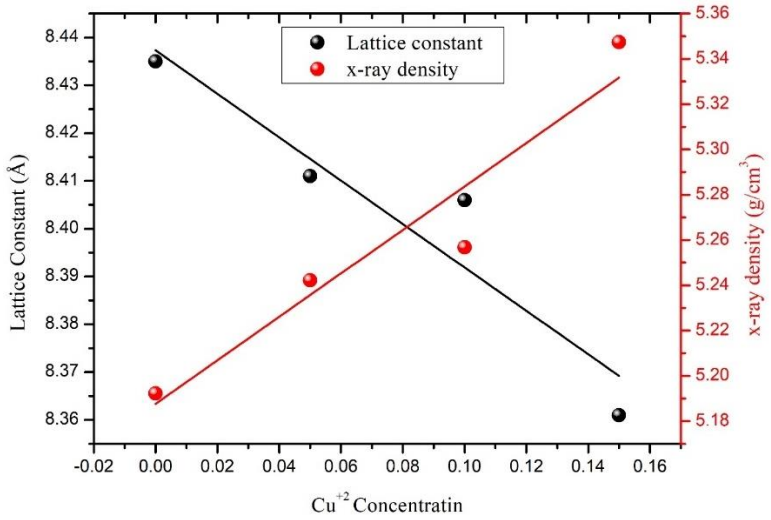

Fig. 2 Variations in the lattice constant (a) and x-ray density (b) as the concentration of Cu^{+2} varies.

Crystallite size and microstrain were calculated based on Equation (4), where the relationship between 4sinθ and β.cos θ (Williamson-Hall plot) was drawn, as shown in Fig. 3. It was discovered that there is an irregular fluctuation in the sizes of crystallites and microstrain as the concentration of copper ions increases, possibly due to the irregular substitution of ions at octahedral and tetrahedral sites [41]. An increased concentration of copper ions could cause them to move towards tetrahedral sites instead of their usual

octahedral sites, leading to a shift in microstrain [29]. Generally, at 0.05, there was a sudden increase in negative values, followed by a subsequent decrease, yet the trend resumed an upward trajectory later, as listed in Table (1).

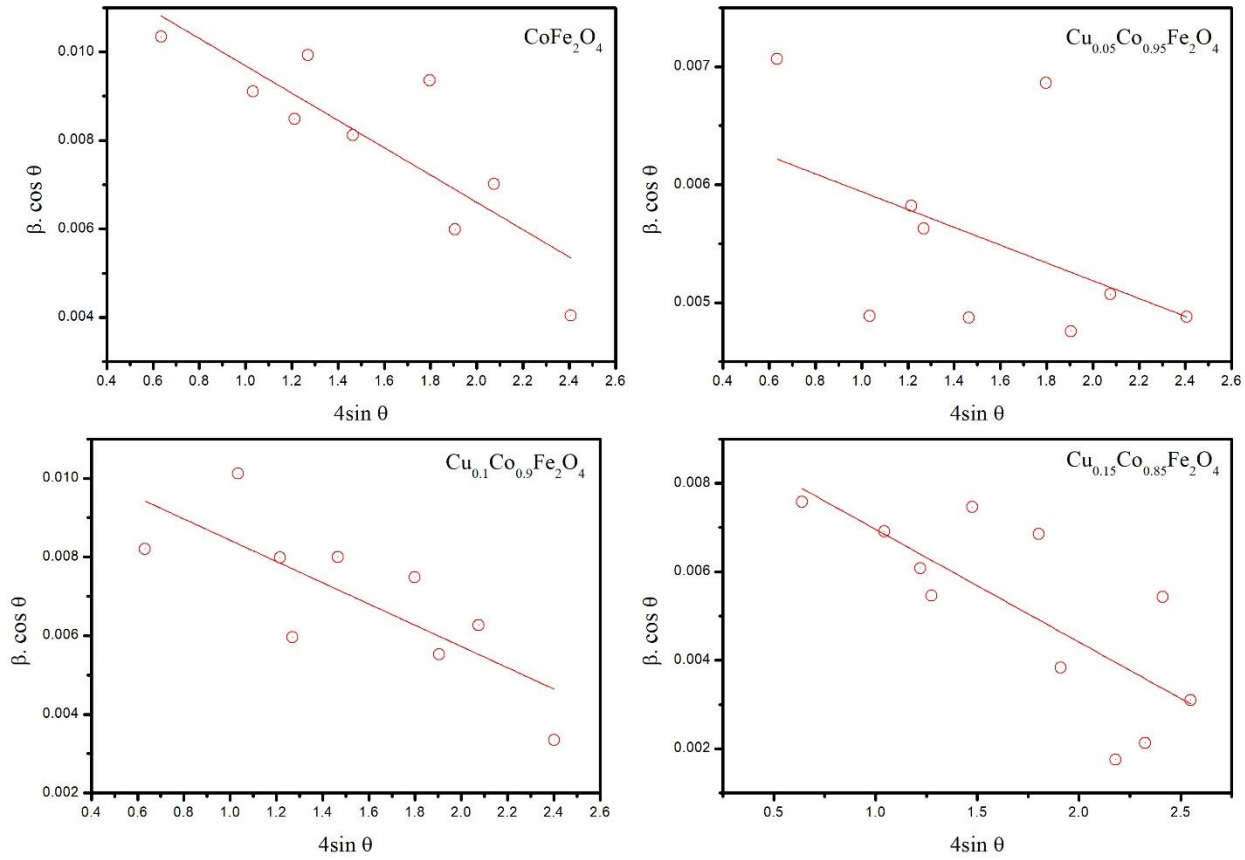

Fig. 3 Williamson-Hall plots of $Cu_xCo_{1-x}Fe_2O_4$ (x=0, 0.05, 0.1 and 0.15).

Table 1: Lattice parameter (a), Crystallite Size (D_{hkl}), microstrain, and X-ray density (d_x) of the synthesized Cu-Co ferrite precursors

Cu^{+2} concentration	a (nm)	D_{hkl} (nm)	Microstrain (%)	d_x (g/cm³)
0	0.8435±0.0038	10.74	-0.00309	5.192
0.05	0.8411±0.0009	20.46	-0.00075	5.242
0.1	0.8406±0.0003	12.32	-0.0027	5.257
0.15	0.8361±0.005	14.42	-0.00255	5.347

Conclusions

The replacement of Cu^{+2} ions has been shown to affect lattice constant, X-ray density, crystal size, and microstrain. This method enables the controlled production of materials with enhanced properties, suitable for various applications including magnetic storage, sensors, electronics, and biomedical devices.

References

1. Dippong, T., Levei, E., & Cadar, O. (2021). Recent Advances in Synthesis and Applications of MFe2O4 (M = Co, Cu, Mn, Ni, Zn) Nanoparticles. Nanomaterials, 4, 1–12.

2. SOUFI, A., HAJJAOUI, H., ELMOUBARKI, R., ABDENNOURI, M., QOURZAL, S., & BARKA, N. (2021). Spinel ferrites nanoparticles: Synthesis methods and application in heterogeneous Fenton oxidation of organic pollutants – A review. Applied Surface Science Advances, 6, 100145. https://doi.org/10.1016/j.apsadv.2021.100145

3. Pacakova, B., Kubickova, S., Reznickova, A., Niznansky, D., & Vejpravova, J. (2017). Spinel Ferrite Nanoparticles: Correlation of Structure and Magnetism. In M. Seehra (Ed.), Magnetic Spinels - Synthesis, Properties and Applications (pp. 3–30). https://doi.org/10.5772/66074

4. Nikam, C. U., Kadam, S. R., Shitole, R. S., Birajdar, A. P., Barote, V. K., Wadgnae, S. R., … Kale, G. H. (2023). Williamson-Hall and Size-strain plot based micro-structural analysis and evaluation of elastic properties of Dy3+substituted Co-Zn nano-spinels. In Journal of Physics: Conference Series (Vol. 2426, p. 012029). IOP Publishing. https://doi.org/10.1088/1742-6596/2426/1/012029

5. Bansal, M., Ahlawat, D. S., Singh, A., Kumar, V., & Rathee, S. P. (2020). Effect of heat treatment on the microstructural properties of silica embedded cobalt ferrite nanocomposites. Nanocomposites, 6(4), 158–164. https://doi.org/10.1080/20550324.2020.1865711

6. Abouhaswa, A. S., Badr, M. H., Nasr, M. H., Elkholy, M. M., El-Deen, L. M. S., Turky, G. M., … EL-Hamalawy, A. A. (n.d.). Investigation of Crystal Structure , Electrical and Magnetic Properties of Spinel Mn-Cd Ferrite Nanoparticles. Journal of Inorganic and Organometallic Polymers and Materials, 32, 486–498.

7. Dedi, Idayanti, N., Kristiantoro, T., Alam, G. F. N., & Sudrajat, N. (2018). Magnetic properties of cobalt ferrite synthesized by mechanical alloying. AIP Conference Proceedings, 1964, 1–5. https://doi.org/10.1063/1.5038285

8. Rao, K. S., Choudary, G. S. V. R. K., Rao, K. H., & Sujatha, C. (2015). Structural and Magnetic Properties of Ultrafine CoFe2O4 Nanoparticles. In 2nd International Conference on Nanomaterials and Technologies (CNT 2014) (Vol. 10, pp. 19–27). Elsevier B.V. https://doi.org/10.1016/j.mspro.2015.06.019

9. Mahdikhah, V., Ataie, A., Babaei, A., Sheibani, S., Yang, C. W. O., & Abkenar, S. K. (2019). Control of structural and magnetic characteristics of cobalt ferrite by post-calcination mechanical milling. Journal of Physics and Chemistry of Solids, 134(June), 286–294. https://doi.org/10.1016/j.jpcs.2019.06.018

10. Prasetya, N. P., Utari, Iriani, Y., & Purnama, B. (2023). The Effect of Annealing Temperature on the Structural and Magnetic Properties of Lanthanum Doped Cobalt Ferrite with the Bengawan Solo River Fine Sediment as the Source of Fe3+. Key Engineering Materials, 940(January), 11–20. https://doi.org/10.4028/p-hr571t

11. Dhaka, S., Kumar, S., Poonia, K., Singh, V., Dhaka, K., & Mund, H. S. (2021). Effect of annealing temperature on structural and magnetic properties of nano-cobalt ferrite.

Journal of Materials Science: Materials in Electronics, 32(12), 16392–16399. https://doi.org/10.1007/s10854-021-06192-y

12. Ibrahim, A. M., El-Latif, M. M. A., & Mahmoud, M. M. (2010). Synthesis and characterization of nano-sized cobalt ferrite prepared via polyol method using conventional and microwave heating techniques. Journal of Alloys and Compounds, 506(1), 201–204. https://doi.org/10.1016/j.jallcom.2010.06.177

13. Rzaij, J. M., Ibraheam, A. S., & Abass, A. M. (2021). Cobalt Effect on the Growth of Cadmium Oxide Nanostructure Prepared by Spray Pyrolysis Technique. Baghdad Science Journal, 18(2), 401–408. https://doi.org/10.21123/bsj.2021.18.2.0401

14. Sdran, N. Al, Shkir, M., & Ali, H. E. (2024). Facile combustion-synthesis, structural, morphological, vibrational, photoluminescence, dielectric, and electrical properties of ZnFe2O4 nanostructures: an effect of citric acid concentrations. Journal of Alloys and Compounds, 993, 174540.

15. Nica, V., Caro, C., P, J. M., Leal, M. P., & Garcia-martin, M. L. (2020). Bi-Magnetic Core-Shell CoFe2O4@MnFe2O4 Nanoparticles for In Vivo Theranostics. Nanomaterials, 10(5), 1–16.

16. Jabbar, R., Sabeh, S., & Hameed, A. (2020). Synthesis and Characterization of CoFe2O4Nanoparticles Prepared by Sol-GelMethod. Engineering and Technology Journal, 38(2B), 47–53. https://doi.org/10.30684/etj.v38i2b.252

17. Jumaa, J. S., Saeed, S. R., & Mohammad, A. M. (2023). Synthesis of CoFe2O4/SiO2 nanoparticles and investigation of their magnetic, dielectric, and structural characteristics. Passer Journal of Basic and Applied Sciences, 5(2), 278–289. https://doi.org/10.24271/PSR.2023.391586.1302

18. Houshiar, M., Zebhi, F., Razi, Z. J., Alidoust, A., & Askari, Z. (2014). Synthesis of cobalt ferrite (CoFe2O4) nanoparticles using combustion, coprecipitation, and precipitation methods: A comparison study of size, structural, and magnetic properties. Journal of Magnetism and Magnetic Materials, 371, 43–48. https://doi.org/10.1016/j.jmmm.2014.06.059

19. Singh, R. K., Rai, B. C., & Prasad, K. (2012). Synthesis and Characterization of Copper Substituted Cobalt Ferrite Nanoparticles. International Journal of Advanced Materials Science, 2(3), 71–76. https://doi.org/10.1063/5.0052392

20. Alahmari, F., Khan, F. A., Sozeri, H., Sertkol, M., & Jaremko, M. (2024). Electrospun Cu-Co ferrite nanofibers: synthesis, structure, optical and magnetic properties, and anti-cancer activity. RSC Advances, 14(11), 7540–7550. https://doi.org/10.1039/d3ra08087k

21. Dippong, T., Levei, E. A., Lengauer, C. L., Daniel, A., Toloman, D., & Cadar, O. (2020). Investigation of thermal, structural, morphological and photocatalytic properties of CuxCo1-xFe2O4 ($0 \leq x \leq 1$) nanoparticles embedded in SiO2 matrix. Materials Characterization. https://doi.org/10.1016/j.matchar.2020.110268

22. Batoo, K. M., Salah, D., Kumar, G., Kumar, A., Singh, M., Abd El-Sadek, M., … Jameel, D. A. (2016). Hyperfine interaction and tuning of magnetic anisotropy of Cu doped CoFe2O4 ferrite nanoparticles. Journal of Magnetism and Magnetic Materials, 411, 91–97. https://doi.org/10.1016/j.jmmm.2016.03.058

23. Ali, B. M., Alsabah, Y. A., Siddig, M. A., Elbadawi, A. A., Ahmed, A. I., & Mirghni, A. A. (2020). Influenced of Cu2+ Doped on Structural, Morphological and Optical Properties of Zn-Mg-Fe2O4 Ferrite Prepared by Sol-Gel Method. Advances in Nanoparticles, 09(02), 49–58. https://doi.org/10.4236/anp.2020.92004

24. Pilania, G., Kocevski, V., Valdez, J. A., Kreller, C. R., & Uberuaga, B. P. (2020). Prediction of structure and cation ordering in an ordered normal-inverse double spinel. Communications Materials, 1(1), 1–11. https://doi.org/10.1038/s43246-020-00082-2

25. Jnaneshwara, D. M., Avadhani, D. N., Daruka Prasad, B., Nagabhushana, H., Nagabhushana, B. M., Sharma, S. C., … Shivakumara, C. (2014). Role of Cu2+ ions substitution in magnetic and conductivity behavior of nano CoFe2O4. Spectrochimica Acta - Part A: Molecular and Biomolecular Spectroscopy, 132, 256–262. https://doi.org/10.1016/j.saa.2014.04.179

26. Ghosh, M. P., & Mukherjee, S. (2019). Microstructural, magnetic, and hyperfine characterizations of Cu-doped cobalt ferrite nanoparticles. Journal of the American Ceramic Society, 102(12), 7509–7520. https://doi.org/10.1111/jace.16687

27. Nasiri, A., Rajabi, S., Amiri, A., Fattahizade, M., Hasani, O., Lalehzari, A., & Hashemi, M. (2022). Adsorption of tetracycline using CuCoFe2O4@Chitosan as a new and green magnetic nanohybrid adsorbent from aqueous solutions: Isotherm, kinetic and thermodynamic study. Arabian Journal of Chemistry, 15(8), 104014. https://doi.org/10.1016/j.arabjc.2022.104014

28. Anju, Yadav, R.S., Pötschke, P., Pionteck, J., Krause, B., Kuřitka, I., Vilčáková, J., Škoda, D., Urbánek, P., Machovský, M. and Masař, M. (2022). Based Thermoplastic Polyurethane Nanocomposites with Reduced Graphene Oxide for Highly Efficient Electromagnetic Interference Shielding, 4.

29. Saleem, S., Irfan, M., Naz, M. Y., Shukrullah, S., Munir, M. A., Ayyaz, M., … Rahman, S. (2022). Investigating the Impact of Cu2+ Doping on the Morphological, Structural, Optical, and Electrical Properties of CoFe2O4 Nanoparticles for Use in Electrical Devices. Materials, 15(10). https://doi.org/10.3390/ma15103502

30. Mohammed, E. A. (2021). A comparative study of the method of Williamson Hall and the pattern of cadmium oxide nanoparticles for X-rays. Turkish Journal of Computer and Mathematics Education (TURCOMAT), 12(4), 881–889. https://doi.org/10.17762/turcomat.v12i4.576

31. Sukumar, M., John Kennedy, L., Judith Vijaya, J., Al-Najar, B., & Bououdina, M. (2018). Facile microwave assisted combustion synthesis, structural, optical and magnetic properties of La2−xSrxCuO4 (0 ≤ x ≤ 0.5) perovskite nanostructures. Journal of

Magnetism and Magnetic Materials, 465, 48–57. https://doi.org/10.1016/j.jmmm.2018.05.094

32. Mittemeijer, E. J., & Welzel, U. (2008). The "state of the art" of the diffraction analysis of crystallite size and lattice strain. Zeitschrift fur Kristallographie, 223(9), 552–560. https://doi.org/10.1524/zkri.2008.1213

33. Jahil, S. S., Mohammed, I. A., Khazaal, A. R., Jasim, K. A., & Harbbi, K. H. (2022). Application the Halder – Wagner to Calculation Crystal Size and Micro Strain by X-ray Diffraction Peaks Analysis. NeuroQuantology, 20(1), 199–204. https://doi.org/10.14704/nq.2022.20.1.nq22074

34. Ali, H. H., & Alalousi, M. A. (2023). Initial Characterization of the Prepared Au-Decorated TiO2:Fullerene Films Using Electrospray Method. Iraqi Journal of Applied Physics, 19(4B), 151–156.

35. Ibraheam, A. S., Rzaij, J. M., & Arshad, M. K. M. (2023). Influence of Magnesium Content on the Structural, Optical, and Electrical Properties of Cu2(Zn1-xMgx)SnS4 Nanostructured Quaternary Thin Film Synthesized Using the Sol–Gel Method. Journal of Electronic Materials, 52(1), 414–421. https://doi.org/10.1007/s11664-022-10002-4

36. Tawfeeq, H. A., & Rzaij, J. M. (2024). The effect of Nb2O5 and pdo nanostructures coating on the structural and morphological properties of CdO thin films. In Iraqi Journal of Applied Physics (Vol. 19, p. 050011). https://doi.org/10.1063/5.0196260

37. Rzaij, J. M. (2023). A novel room-temperature nitrogen dioxide gas sensor based on silver-doped cerium oxide thin film. Sensors and Actuators A: Physical, 363, 114748. https://doi.org/10.1016/j.sna.2023.114748

38. Barkat, F., Afzal, M., Khan, B. S., Saeed, A., Bashir, M., Mukhtar, A., … Wu, K. (2022). Formation Mechanism and Lattice Parameter Investigation for Copper-Substituted Cobalt Ferrites from Zingiber officinale and Elettaria cardamom Seed Extracts Using Biogenic Route. Materials, 15(13). https://doi.org/10.3390/ma15134374

39. Abu-Elsaad, N. I., & Nawara, A. S. (2024). Effect of Cu substitution on magnetic and photocatalytic properties of Mn–ZnFe2O4 nanoparticles. Journal of Materials Science, 59(10), 4167–4185. https://doi.org/10.1007/s10853-024-09486-8

40. Farooq, W. A., Sajjad Ul Hasan, M., Khan, M. I., Ashraf, A. R., Abdul Qayyum, M., Yaqub, N., … Hani, A. (2021). Structural, optical and electrical properties of Cu0.6CoxZn0.4-xFe2O4 (x = 0.0, 0.1, 0.2, 0.3, 0.4) Soft Ferrites. Molecules. https://doi.org/10.3390/molecules26051399

41. Rzaij, J. M., Abbas, Q. A., & Khalaf, A. M. (2023). Investigating the structural, topographical, morphological and optical effects of AgO on sprayed SnO2 thin films. Bulletin of Materials Science, 46(4), 200. https://doi.org/10.1007/s12034-023-03040-z

IRAQI Academic Scientific Journals
Samarra Journal of Pure and Applied Science
SJPAS
مجلة سامراء للعلوم البحتة والتطبيقية
www.sjpas.com
p ISSN: 2663-7405
e ISSN: 2789-6838

تأثير محتوى النحاس على الخصائص التركيبية لفريت الإسبنيل النانوي $Cu_xCo_{1-x}Fe_2O_4$ بناءً على تحليل ويليامسون-هول

مرام جدوع حسن[1]، نزار عصمت سينو[2]، مازن عبد الحميد الآلوسي[3]، جمال مال الله رزيج[3]*
1- قسم علوم الحاسوب، كلية التربية الأساسية، الجامعة المستنصرية، العراق
2- مركز الطاقة المتجددة، جامعة الأنبار، العراق
3- قسم الفيزياء، كلية العلوم، جامعة الأنبار، الرمادي، العراق

معلومات البحث:
تأريخ الاستلام: 2023/07/02
تاريخ التعديل : 2023/08/05
تأريخ القبــول: 2023/08/08
تاريخ الـنشر: 2024/12/30
الكلمات المفتاحية:
فيرايت النحاس-كوبلت، الفرايت الشوكي، ويليامسون-هول، الخواص التركيبية، الفرايت النانوي

معلومات المؤلف
الايميل:
sc.jam72al@uoanar.edu.iq
الموبايل:

الخلاصة:
بحثت الدراسة الحالية في تأثير استبدال ايونات الكوبالت (Co^{+2}) بـايونات النحاس (Cu^{+2}) لتعديل الخصائص الفيزيائية للمركب النانوي $Cu_xCo_{1-x}Fe_2O_4$ عند قيم اكس 0، 0.05، 0.1، و0.15 المرسبة باستخدام طريقة احتراق الـجل-هلام. تم إجراء التحليل التركيبي باستخدام أنماط حيود الأشعة السينية وطريقة ويليامسون هول. كشفت الأنماط عن تركيب متعدد التبلور من الفريت دون وجود قمم مميزة مرتبطة بالنحاس. كان الطور السائد للنمو البلوري باتجاه قمة الحيود (311) مع تحول ملحوظ لقمم الحيود باتجاه زاوية الحيود المنخفضة مع زيادة محتوى النحاس. لوحظ انخفاض ثابت الشبيكة البلورية بينما ازدادت شدة قمم الحيود مع ارتفاع محتوى النحاس. أظهرت الدراسة ان الغشاء المحضر ذو ثابت شبيكة بلورية 0.8361 ± 0.005 نانومتر بكثافة أشعة سينية تبلغ 5.347 جم/ سم3 للـعينة ذات x = 0.15. بالإضافة إلى ذلك، لوحظ تباين الحجم البلوري من 10.74 نانومتر إلى 20.46 نانومتر بينما تغير الاجهاد من -0.00255% إلى -0.00309% مع تغيير نسبة محتوى x.